A powerful scanning methodology for 3D measurements of small parts with complex surfaces and sub millimeter-sized features, based on close range photogrammetry

Title. A powerful scanning methodology for 3D measurements of small parts with complex surfaces and sub millimeter-sized features, based on close range photogrammetry.

Author names and affiliations. L. M. Galantucci[a], M. Pesce[a], F. Lavecchia[b]

[a]Politecnico di Bari, Dipartimento di Meccanica, Matematica e Management, Viale Japigia 182, Bari 70126, Italy

[b]Polishape 3D srl, Dipartimento di Meccanica, Matematica e Management, Viale Japigia 182, Bari 70126, Italy

Abstract. A powerful and cost effective photogrammetric scanning methodology, suitable for reconstructing a full 3D digital model of parts with complex surfaces and sub millimeter-sized features, is described. The scanner employed for this purpose is composed of a computerized system that drives and control the movements of a rotary table, and a digital SLR camera for the images acquisition. The object is positioned on the rotary table that rotates at fixed angles, while the digital camera, mounted on the stator through a rigid frame, captures the images. The scanning process has been optimized with the aim to minimize the number of shots and thus, the time needed to obtain a complete 3D digital model, which is not dependent from the dimensions of the object. With the aim to demonstrate the effectiveness of the proposed scanning methodology, four benchmarks have been realized to provide complex examples. The 3D digital models were compared with those obtained with an Optimet™ Conoscan 4000 which uses a conoscopic holographic sensor.

Keywords. Close-range photogrammetry, non-contact system, 3D digital model, 3D measurements, sub-millimeter, complex surfaces.

1. Introduction

Due to the availability of current ultra-precise milling centers which enable to machine parts with accuracy ranging from 1 µm to 0.01 µm [1] and to the development of new manufacturing technologies for the production of micro components [2–5], the demand of measuring instruments for small parts has been strongly supported. In fact, there is an increasing need to perform three-dimensional measurements of objects with complex surfaces and sub millimeter features, such as the molds for the process of micro injection molding or the tools used in the process of micro EDM.

Currently, there are several technologies to meet the arising metrological needs [6]. According to a recent classification [7], the most suitable technology for the measurement of three-dimensional objects with complex surface and sub millimeter features, would be X-ray computer tomography [8]. X-ray computer tomography is widely used for various micro and nano-metrology applications such as the measurement of MEMS [9], the analysis of the scaffolds [10], the inspection of diesel nozzle orifices [11], or to perform non-destructive test for defects inspection [7]. Coordinate measuring machines (CMM) are also widely used for that purpose [13], however, they are generally expensive and large in size. Although some economic and compact CMM system are being developed [14,15], the tactile and optical CMM instruments presents some limitations. When small and delicate objects with complex shape must be measured, mechanical probing causes elastic and plastic deformations at the contact point, and the measurable point rate is quite low [16–18]. On the other hand, optical probing systems do not deform the object and have high point rate, but they have limitations in measuring high surface slopes and problems related to the diffraction limit of lateral resolution [18,19] and to the transparency of the object [7]. In addition, both CMM and X-ray tomography, are not able to return a 3D model with the object natural color texture. In [7], the authors state that photogrammetry would not be suitable for small parts and complex surfaces. Instead, in recent works [20,21] other authors demonstrated that it is possible to use photogrammetry in order to obtain accurate 3D models of small object (maximum dimensions between 30 mm and 3 mm) and in sub millimeter scale [22].

2. Materials and methods

This paper presents a performing and low-cost Photogrammetric Scanning System with Rotary Table (PSSRT), capable to return precise 3D digital models of objects a few millimeters long, which presents complex surfaces and sub-millimeter features. The work has been carried out in parallel to that reported in [21], however, significant improvement in terms of shooting technique, acquisition times, quality and precision of measurements have been achieved. In fact, analyzing the shots captured by the presented PSSRT (Figure 1), it is possible to state that the percentage of the frame occupied by the object is about 90%, compared to 30% - 40% used in [21]. A greater coverage percentage allows to increase the rate between digital model precision and the computational work [23]. This condition enables us to get a complete 3D digital model using only 36 frames instead of 144 frames (up to 4464 in macro mode) used in [21]. Consequently, the proposed scanning methodology enables to save time in the photos acquisition process as well as in the photos processing: the duration of a full acquisition is about 5 minutes, while the photos processing time is approximately 10 minutes. Finally, it was possible to obtain 3D digital models in 1:1 scale with high dimensional accuracy, thanks to the use of a reference scale measured on a single feature with a caliper or a CMM machine.

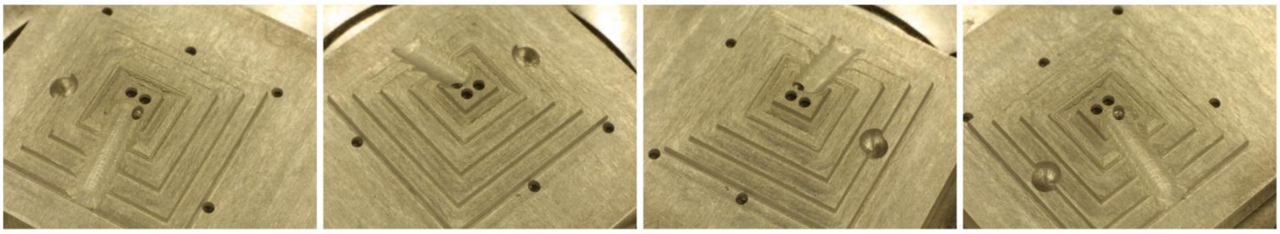

Figure 1: Some pictures taken with the proposed PSSRT, during the scan of the sample named "Pyramid 1".

2.1. Realization of the test

To validate the proposed PSSRT, four benchmarks named Pyramid 1, Pyramid 2, Pyramid 3 and Pyramid 4, with complex surface and sub millimeter features have been realized. The samples were made in aluminum alloy, and have been machined on a 3-axes machining center. In Table 1, a detailed description of the characteristics of the benchmarks is proposed.

Table 1: Nominal dimensions of the specimens features.

	Pyramid 1	Pyramid 2	Pyramid 3	Pyramid 4
Base in mm	20X20	24X24	24X24	12X12
Step height in mm	1.0	0.5/0.25	0.20	0.02
# Steps	5	5+1	6	6
Total height in mm	5.0	2.75	1.2	0.4
Radius of smaller holes in mm	0.6	0.6	0.6	0.6
Depth of smaller holes in mm	1.3	0.85	1.35	0.35
Radius of the big hole in mm	1.5	1.5	1.5	0.85
Angulation of the walls with chamfer in degree	45	45	45	40
Width of the slot in mm	-	0.5	0.5	0.6
Depth of the slot in mm	-	0.1	0.1	0.1

The samples are geometrically similar to those used in several works to calibrate a scanning system based on the acquisition of stereo SEM (Scanning Electron Microscopes) images for photogrammetric applications [24 - 28]. The pyramidal geometry, and the presence of various features such as holes of different sizes, chamfers and grooves, make the samples particularly useful to test the suitability of the proposed PSSRT, to scan objects with complex surfaces and sub millimeter features. Moreover, the total height of each benchmark is different, and this allows to appreciate the depth of field capability of the proposed PSSRT. Finally, applying this methodology to metallic parts, a simple chemical etching can be performed, useful for dull surfaces and limit the problems arising from the high reflectivity of metals. The aluminum samples were immersed in a sodium hydroxide solution (20%$_W$) properly flustered by an agitator for about 90 s. The process parameters set in this way allows to remove only a negligible amount of material.

2.2. The proposed Photogrammetric Scanning System (PSSRT)

For the realization of the PSSRT a digital SLR camera Canon 40D (Effective pixels 10 megapixels, Sensor size APS-C 22.2 x 14.8 mm) with Canon EF 50 mm 1:1:8 II lens and Kenko Extension Tubes were used. The PSSRT has been developed in order to automate and improve the traditional technique for photogrammetric reconstructions, in which the object is stationary in a certain position and the operator takes pictures around it. On the contrary, the working principle of the proposed PSSRT, requires that the object is placed on a rotary table (D) designed and built specifically for scanning small objects (up to 50x50 mm) and rotates, while a Digital SLR Camera (A), is fixed on a platform (B) which can be moved along a rigid tubular frame (C) (Figure 2).

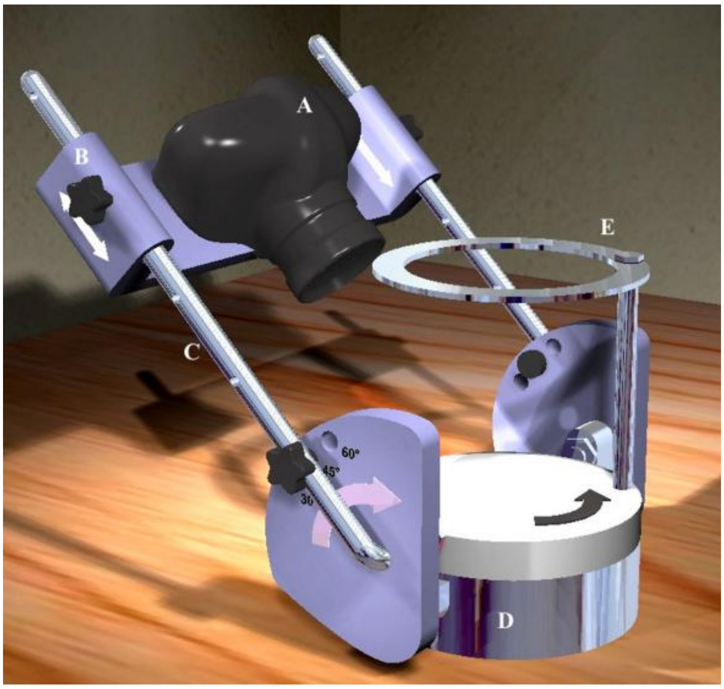

Figure 2: Design of the proposed PSSRT: A) Digital SLR Camera; B) Platform for focus distance tuning; C) Rigid tubular frame for tilt angle tuning; D) Rotary Table; E) Light.

After the object has been positioned at the center of the turntable, the camera distance from the object has to be tuned, in order to regulate the focus. The focus distance of the lens (mounted on the extension tube) is set to infinity, thus it is necessary to regulate the distance from the object, which is unique for a particular configuration of the lens/extension tube length, in order to get the object in focus. This criterion allows to get photographs with negligible distortion and therefore greater precision in reconstructing the 3D digital model, even without a proper internal camera calibration, since the camera lenses are manufactured with the aim to minimize the distortions in the image when focuses to infinity. This solution was preferred respect with the use of a macro lens (which would be ideal for taking photos distortion-free at close range), with the aim to propose a versatile scanning system while fixing the focal length, which is and essential condition for the future developments about the camera calibration issue. Depending from the size of the object, it is possible to increase or restrict the field of view (move away or move closer the camera from the object) just choosing a different extension tube length and positioning the digital camera at the correct distance from the object. In the present work the 50 mm camera lens was used with a 36 mm extension tube length. Then the tilt angle of the camera (incident rays) should be adjusted. The proposed PSSRT allow to set the camera at 30°, 45° or 60° from the horizontal. The tilt angle depends on the geometry of the object to be scanned. For example if the object presents some holes on his top surface, the tilt angle should be set in order to allow the penetration of the incident rays inside the holes, and this will enable to reconstruct the internal wall of the same. The tubular rigid frame of the PSSRT has been design to constrain the camera to move in a circular path, with radius equal to the distance from the object (which has been fixed in the step before) and the center coinciding with the center of the turntable. In this manner the focusing point will not change varying the tilt angle. The acquisitions performed with the PSSRT and used to realize the 3D digital models reported in the present work have been done at 60° tilt angle. Moreover, a LED light source (E in Figure 2) integral with the rotor of the turntable, ensures uniform and homogeneous lighting during the rotation. The lighting intensity can be easily adjusted just translating the light source along the vertical axis. The acquisition step is fully automated and controlled remotely from a computer: the turntable rotates of 10°, then stops, a shutter trigger is sent to the camera, and the frame is acquired. The rotation angle chosen, allows to achieve a good overlap of the frames and thus to obtain a good result, using only 36 images. This operation is repeated until the turntable has completed a whole 360° turn. Then, the images are processed using an image-based 3D modeling software, which employ the Structure-From-Motion (SFM) and Dense Multi-View 3D Reconstruction (DMVR) algorithms, to build 3D models by unordered image collections that depict a scene or an object from different viewpoints [29]. The procedure of photographs processing and 3D model construction starts with the alignment step, during which the software detects common points in the source photos and matches them with a SIFT (Scale-invariant feature transform) like approach [30]. Furthermore, during the alignment, the position of the camera in the 3D space is computed for each picture. The sparse point cloud represents the results of photo alignment and will not be directly used in the further 3D model construction procedure. On the contrary, the set of camera positions is required for the next step, which is the dense points cloud building, constructed on the basis of the estimated camera positions and pictures themselves and using the pair-wise depth map computation algorithm. Afterwards a 3D polygonal mesh, representing the object surface, is computed by the software on the basis of the dense point cloud. Finally, after the mesh has been reconstructed, the 3D digital model can be textured [31].

2.3. The conoscopic scanner, used as reference

To compare the acquisition done with the proposed PSSRT, an Optimet™ Conoscan 4000 (OC 4000) conoscopic laser scanning system was used. This is a 3-axes scanner which uses conoscopic holography sensors, suitable to perform 3D measurement of objects with complicated geometries, with dimensions up to 160 x 150 mm. The working principle of this scanner is based on the measurement of the interference between the two beams generated after a light beam has gone through an optically anisotropic crystal [32]. Interchangeable sensors and replaceable objective lenses allow a precise tuning of the system to specific applications. For this work an HD sensor was used with a 50 mm objective lenses, which enable to perform 3D measurement with 2 mm working range, precision of 2.5 μm and repeatability 3σ of 0.5 μm.

3. Results

The benchmarks were scanned using both the proposed PSSRT and the OC 4000. The models obtained with the conoscopic scanner have been used as a reference objects to evaluate the performance of the proposed PSSRT. In Figure 3 a comparison among a perspective picture of the benchmark named Pyramid 1 and the related 3D digital models obtained with both scanning systems, is proposed. The 3D digital models of

Pyramid 2, Pyramid 3 and Pyramid 4 have been reported in the Appendix (Figure A1, Figure A2 and Figure A3 respectively).

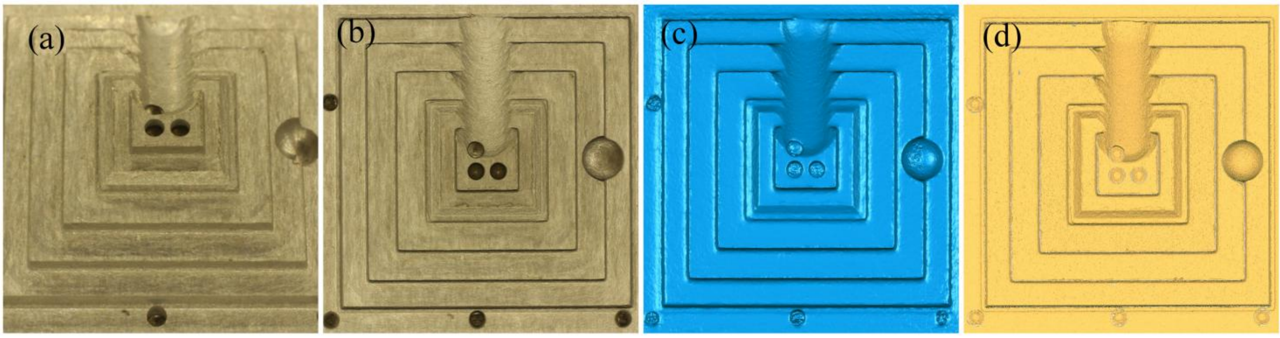

Figure 3: Images related to Pyramid 1: (a) Perspective picture, (b) Texturized 3D digital model obtained with PSSRT, (c) non-texturized 3D digital model obtained with PSSRT, (d) 3D digital model obtained with Optimet™ Conoscan 4000.

The texturized model in Figure 3(b) compared to the perspective picture of Pyramid 1in Figure 3(a) results very realistic, while the non-texturized model in Figure 3(c) allow to appreciate the goodness of the result compared with the digital model in Figure 3(d). It is important to highlight that the lens used in order to obtain the model in Figure 3(d) allow to scan with 2 mm working range; as the total height of Pyramid 1 is 5 mm (Table 1), it was necessary to perform three scans by positioning the Optimet™ conoscopic sensor at three different distances from the object, and align them in order to obtain the complete digital model of the considered benchmark. Otherwise, with the proposed PSSRT, it was possible to obtain the whole model shown in Figure 3(b)-(c), in few minutes with a single scan.

3.1. Uncertainty evaluation of PSSRT

In this section, has been evaluated a quantitative variable to state the reliability and quality of the measurements which can be performed on a 3D digital model built with the PSSRT. This variable is expressed in terms of uncertainty $u(\bar{x})$, and is calculated according with the international standard ISO ENV 13005 ("Guide to the expression of uncertainty in measurement (GUM)"), by the statistical analysis of a sets of observations (A Category) (1), where $s_{\bar{x}}$ is the standard deviation of the mean, s_x is the sperimental standard deviation calculates as the square root of the variance (2) and N is the number of observations. The variable $\bar{x}$ in (2) is the arithmetic mean of the measurements.

$$u(\bar{x}) = s_{\bar{x}} = \frac{s_x}{\sqrt{N}} \tag{1}$$

$$s_{\bar{x}}^2 = \frac{s_{\bar{x}}^2}{N} = \frac{1}{N \cdot (N-1)} \sum_{j=1}^{N} (x_j - \bar{x})^2 \tag{2}$$

With this purpose, 10 stochastically independent scans of the specimen Pyramid 1 were performed under controlled conditions. Then, the 3D digital models have been built as previously described, manually scaled giving the same value for the diagonal of the basis, aligned with each other and sectioned with three planes in order to obtain three curves (S1, S2 and S3) for each model. The curves S1 and S2 have been created using an XZ plane with the aim to measure the total height of the specimen (F1) and a feature along X-axis (F2) respectively, while S3, has been obtained sectioning the digital model with a YZ plane with the aim to measure a feature along Y-axis (F3). The curves S1, S2 and S3 as well as the measurement of the features F1, F2 and F3 have been reported in the Appendix (Figure A4, Figure A5 and Figure A6 respectively).

The values related to the measurements of the three features, with the computed means, the standard deviations and the uncertainties, have been reported in Table 2.

Table 2: Data obtained from the measurements performed on 10 digital models of Pyramid 1 built with the PSSRT.

Name	$\bar{x}$ ***in mm***	s_x ***in mm***	$u(\bar{x})$ ***in mm***
F1	16.3139	$0.7 \cdot 10^{-3}$	$0.2 \cdot 10^{-3}$
F2	16.3041	$1.3 \cdot 10^{-3}$	$0.4 \cdot 10^{-3}$
F3	5.0236	$0.8 \cdot 10^{-3}$	$0.2 \cdot 10^{-3}$

Three Dimensional Comparisons

To evaluate the performance of the proposed PSSRT, 3D-comparisons were performed. This analysis computes the 3D deviations as the distance from the Test to any point on the Reference object surface. As a result of the 3D-comparisons, in Figure 4 are given the color maps representing the 3D deviations between the test (model obtained with the proposed PSSRT) and the reference object (models obtained with the OC 4000). In green were highlighted the areas in which the deviation is within ± 0.01 mm range. The positive deviations greater than +0.01 mm, were highlighted in yellow, orange and red, while the negative deviations less than -0.01 mm were highlighted in blue and light blue. As can be seen, most of the areas were highlighted in green, and the Gaussian distribution of the 3D deviations indicates a great concentration of them in ± 0.01 mm range. The areas with deep holes have proved to be the most critical and were highlighted in yellow, orange and red.

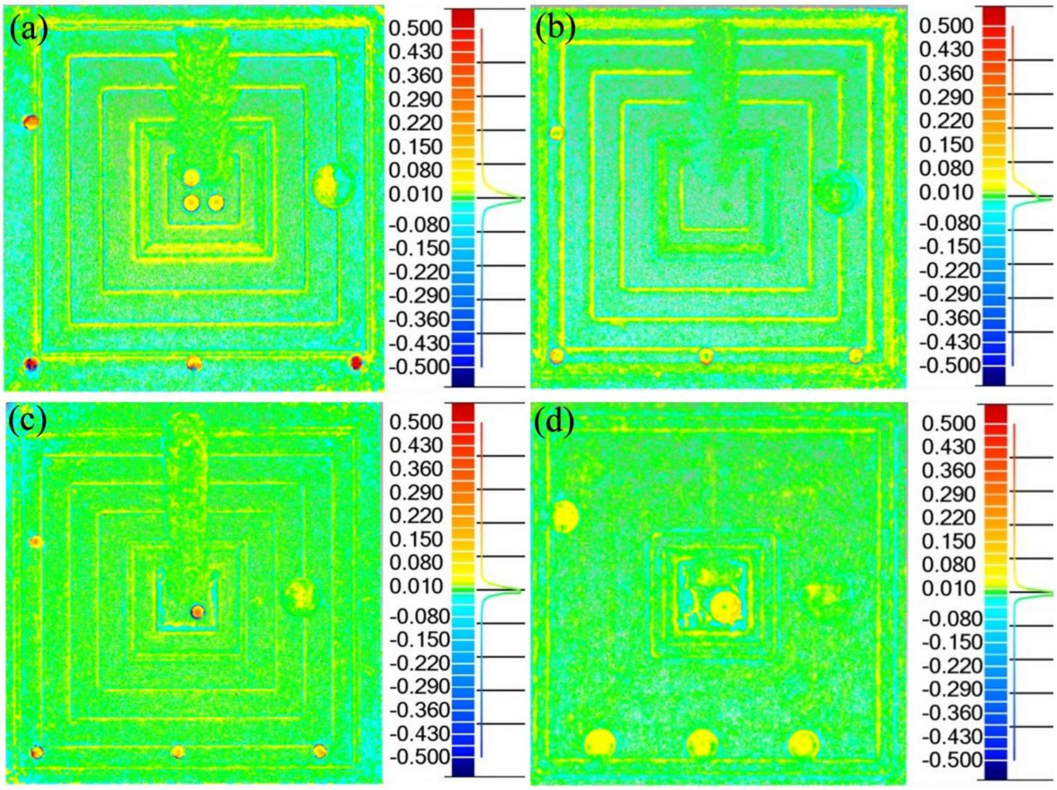

Figure 4: The 3D-comparisons between the models of (a) Pyramid 1, (b) Pyramid 2, (c) Pyramid 3, (d) Pyramid 4, obtained with the proposed PSSRT and the Optimet™ Conoscan 4000 (the color scales are expressed in millimeters).

In Table 3 have been reported the average of the positive distances (Positive Avg), the average of the negative distances (Negative Avg) and the average distance in percentage (Average in %) computes using the equation (3), between the test and the reference model, as well as the standard deviation of all distances of the 3D-comparison.

$$\text{Average in \%} = \frac{(|\text{Positive Avg}|+|\text{Negative Avg}|)/2}{\textit{Diagonal of the basis}} * 100 \quad (3)$$

Table 3: Average distance and standard deviation of all distances computed in the 3D-comparison for each specimen. The values marked with " * ", have been calculated excluding the internal surfaces of deep holes.

	Pyramid 1	*Pyramid 2*	*Pyramid 3*	*Pyramid 4*
Positive Avg in mm	+0.053	+0.025	+0.027	+0.012
Negative Avg in mm	-0.039	-0.014	-0.024	-0.008
Average in %	0.16	0.06	0.08	0.06
Standard deviation in mm	0.099	0.040	0.074	0.016
Positive Avg* in mm	+0.031	+0.019	+0.010	+0.008
Negative Avg* in mm	-0.029	-0.011	-0.011	-0.007
Average* in %	0.11	0.04	0.03	0.04
Standard deviation* in mm	0.059	0.022	0.018	0.011

Two Dimensional Comparisons

With the aim to evaluate the dimensional and shape accuracy of the 3D digital models obtained with the proposed PSSRT respect to that obtained with the OC 4000, a 2D-analysis was carried out. With this purpose, each 3D digital model obtained with the proposed PSSRT was aligned to the related 3D digital model obtained with the OC 4000, and then were sectioned in couple with two planes. The first one, named Section 1, is a XZ plane passing through the center of the groove, while the second one named Section 2, is a YZ plane passing through the diameter of the holes on the upper step of the specimen (Figure 5). In this way, two curves were created and compared for each section, for all the digital models of the four benchmarks.

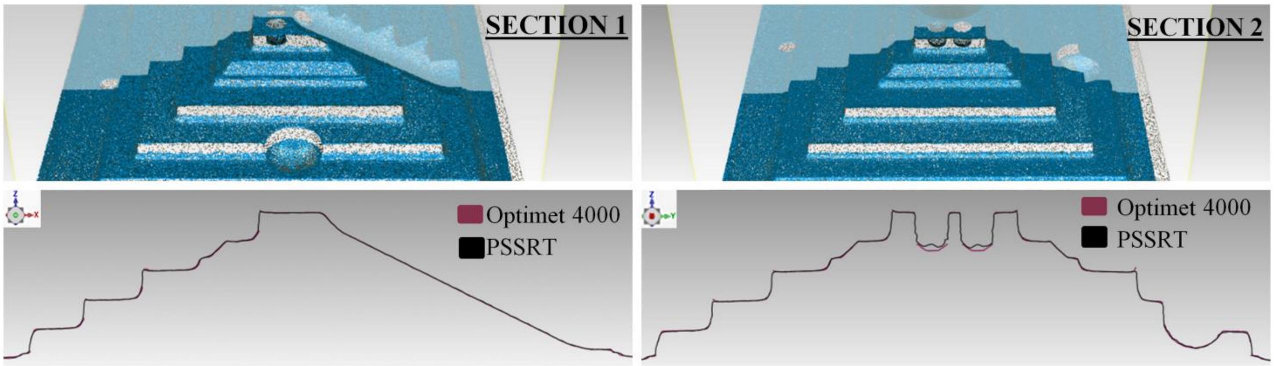

Figure 5: Section planes and related curves created on the 3D digital model of Pyramid 1.

Below have been reported the 2D-comparison carried out for Pyramid 1 in the Section 1 (Figure 6) and in the Section 2 (Figure 7). This analysis calculates the distances between the corresponding points of the two curves created in each section. In green were highlighted the areas in which the distance is within ± 0.01 mm range. The positive deviations greater than +0.01 mm, were highlighted in yellow, orange and red, while the negative deviations less than -0.01 mm were highlighted in blue and light blue. As can be seen in Figure 6 and in Figure 7, the Gaussian distribution of the points distances indicates a good concentration of them within the ±0.01 mm range. The areas with deep holes have proved to be the most critical and were highlighted in red.

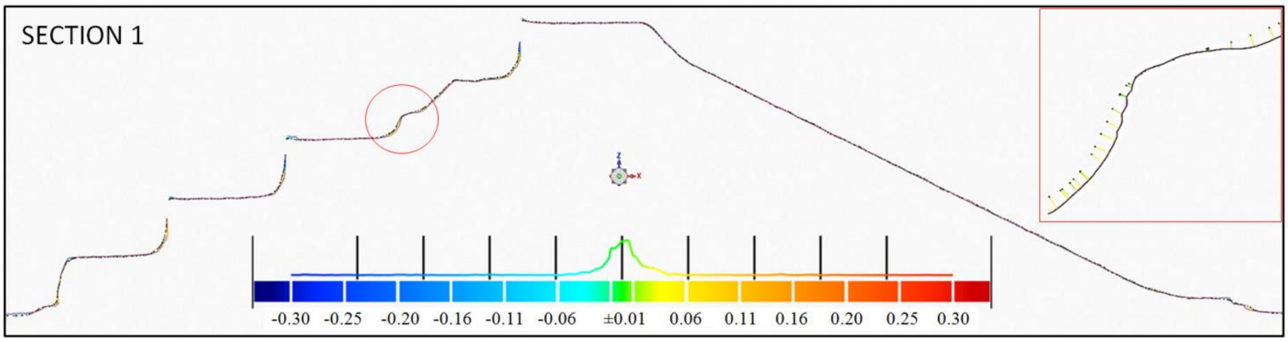

Figure 6: 2D comparison carried out for Pyramid 1 in Section 1. The color scale is expressed in millimeters.

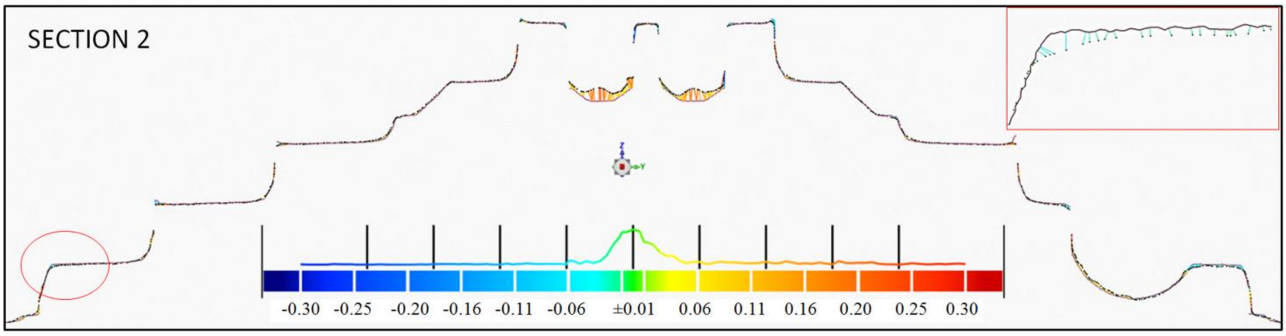

Figure 7: 2D comparison carried out for Pyramid 1 in Section 2. The color scale is expressed in millimeters.

As a demonstration, only the 2D-comparison carried out for the specimen named Pyramid 1 has been reported in the present work. The results of the two-dimensional analysis performed for the two sections of the four benchmark digital models have been reported in Table 4, and are expressed for each section as the average of the positive distances (Positive Avg), the average of the negative distances (Negative Avg) and the average distance in percentage (Average in %) computes using the equation (3), between the corresponding points of the compared curves, as well as the standard deviation of all distances of the 2D-comparison. Thus, the less is the average distance, the less would be the difference in terms of dimensions and shape of the curve created sectioning the 3D digital model obtained with the proposed PSSRT respect to that created sectioning the 3D digital model obtained with the OC 4000.

Table 4: Average distance and standard deviation of all distances computed in the 2D-comparison for each specimen.

	Pyramid 1	*Pyramid 2*	*Pyramid 3*	*Pyramid 4*
Positive Avg in Section 1 in mm	+0.017	+0.014	+0.009	+0.020
Negative Avg in Section 1 in mm	-0.021	-0.011	-0.010	-0.010
Average in Section 1 in %	0.07	0.04	0.03	0.09
Standard deviation in Section 1 in mm	0.042	0.022	0.014	0.026
Positive Avg in Section 2 in mm	+0.050	+0.019	+0.017	+0.019
Negative Avg in Section 2 in mm	-0.025	-0.016	-0.014	-0.010
Average in Section 2 in %	0.13	0.05	0.05	0.09
Standard deviation in Section 2 in mm	0.068	0.027	0.033	0.025

3.2.Two Dimensional Measures

The curves created by sectioning the 3D digital models with the plane Section 2, were used to measure some of the features which have been reported in Table 1. In particular the step height of the samples Pyramid 1, Pyramid 2 and Pyramid 3 were measured. The measurements were performed by taking the vertical distance (along Z axis) between the horizontal step profiles. Due to the elastic recovery of the material that occurs immediately after the passage of the tool during the machining, the horizontal profile of the specimens is not perfectly parallel to the Y axis. Thus, for the measurement of the height of the step, each horizontal profile was approximated by a segment drawn considering the average value of the Z coordinate of all the points of the horizontal step profile (Figure 1Figure 8).

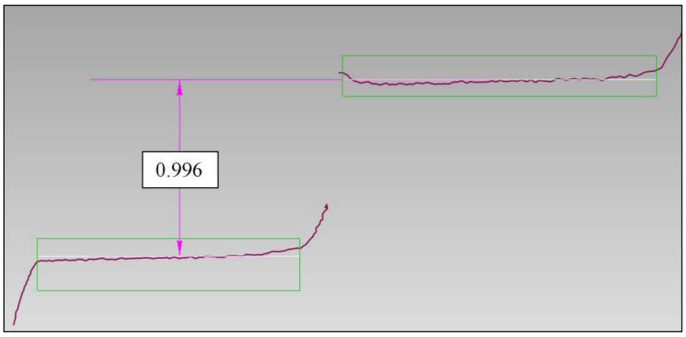

Figure 8: Example of the procedure for the step height measurement.

In order to eliminate the uncertainty related to the user who performs this operation, five independent measurements were taken for each feature. In Table 5 have been reported the measurements of the height of the five step of Pyramid 1, taken on the 3D digital models obtained respectively with the OC 4000 and the proposed PSSRT. The feature H1 refers to the measure of the height of the base step, while H6 refers to the measure of the top step of the pyramid. As the specimen Pyramid 1 has five steps, for this sample the feature H5 refers to the measure of the top step of the pyramid.

Table 5: Measurements performed on the 3D digital model of Pyramid 1 obtained with Optimet™ Conoscan 4000 and the proposed PSSRT.

Name	***Optimet***		***PSSRT***	
	Mean in mm	*Std. Dev. in mm*	*Mean in mm*	*Std. Dev. in mm*
H1	1.007	0.001	1.007	0.001
H2	0.995	0.001	1.000	0.001
H3	0.996	0.001	1.003	0.002
H4	1.012	0.001	1.016	0.002
H5	0.964	0.001	0.962	0.002

The mean of the five measurements carried out for each feature proved to be a good estimator of the actual value, since the standard deviation is within 0.001 mm – 0.002 mm range, for all the measurements performed for the considered samples. Therefore, the measure of the height of a step is given by the mean of the five measurements. In Table 6 have been reported the height of the steps measured using the procedure described above.

Table 6: Measurements of the step height of the 3D digital models of Pyramid 1, Pyramid 2 and Pyramid 3 obtained with Optimet™ Conoscan 4000 and the proposed photogrammetric scanning system.

Name	Pyramid 1			Pyramid 2			Pyramid 3		
	Optimet in mm	PSSRT in mm	Difference in mm	Optimet in mm	PSSRT in mm	Difference in mm	Optimet in mm	PSSRT in mm	Difference in mm
H1	1.007	1.007	0.000	0.501	0.506	0.005	0.195	0.191	0.003
H2	0.995	1.000	0.005	0.494	0.496	0.002	0.197	0.195	0.002
H3	0.996	1.003	0.007	0.504	0.503	0.001	0.202	0.201	0.001
H4	1.012	1.016	0.004	0.507	0.506	0.001	0.200	0.204	0.004
H5	0.964	0.962	0.002	0.525	0.526	0.001	0.194	0.202	0.009
H6	-	-	-	0.223	0.223	0.000	0.315	0.312	0.003

4. Discussion

The preliminary analysis for the estimation of the measurement uncertainty, conducted in agreement with the international standard ISO ENV 13005, has shown that it is possible to perform measurements on 3D digital models obtained with the PSSRT, with a sub micrometer uncertainty (0.2 µm – 0.4 µm). The standard deviation of data is 1.0 µm, that means the 68.3% of the measurement will fall within +/- 1.0 µm range (+/- σ), thus the 99.7% of the measurement will fall within +/- 3.0 µm range (+/- 3σ).

The color maps relative to the 3D-comparisons return excellent results: the Gaussian distributions of the distances show an high concentration of data within the range of ± 0.01 mm. The highest standard deviations are 0.099 mm for Pyramid 1 and 0.074 mm for Pyramid 3, which have the deepest holes (1.3 mm and 1.35 mm respectively – See Table 1), while Pyramid 2 and Pyramid 4 which have shallower holes, shown less data dispersion. The Standard deviation* reported in Table 3 confirm the great influence of such features on the data dispersion, especially for Pyramid 1 and Pyramid 3. Anyway, the highest Positive Avg* (+0.031 mm) and Negative Avg* (-0.029 mm) have been measured for Pyramid 1, and represent a percentage distance between the reference and the test of 0.11% on the whole 3D model, with a standard deviation of 0.059 mm.

To understand the goodness of the result, a little area of 6 x 4.5 mm of Pyramid 1 has been scanned with a microscope that uses the focus variation technology and suitable for this type of applications. The partial 3D digital model obtained with the focus variation microscope was compared with the same portion of the 3D digital model of Pyramid 1 obtained with Optimet™ Conoscan 4000 (Figure 9). The Gaussian distribution of the deviation values shows a greater dispersion of the data: the majority of the values, in fact, is comprised in a range of ±0.08 mm. The average deviation is +0.054 mm / -0.055 mm (in percentage 0.70%), while the standard deviation is 0.092 mm.

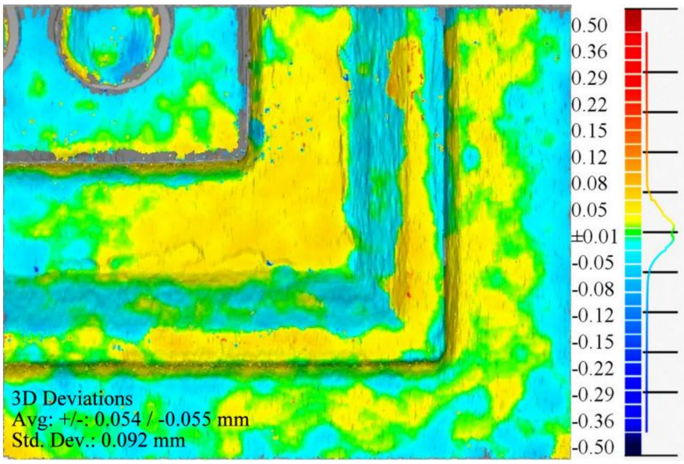

Figure 9: 3D comparison between a portion of the 3D digital models of Pyramid 1, obtained with the focus variation microscope and the Optimet Conoscan 4000. The color scale is expressed in millimeters.

The 2D-comparisons also highlighted the weakness of the proposed PSSRT, related to the scan of the interior of the deepest holes. In fact, these analysis carried out for Section 2 show higher distances between the reference and the object as well as higher standard deviations respect to that carried out for Section 1. This is because the Section 2 has been created in correspondence of the deepest holes on the top step of the specimens and thus take into account such features in the comparisons. Should be noted that the average distances and standard deviation measured for Pyramid 4 do not vary from Section 1 to Section 2 because the holes are not so deep like that of the other specimens. In Figure 10 is given a magnification of the 2D-comparison, carried out for "Section 2" of Pyramid 1, which results particularly significant.

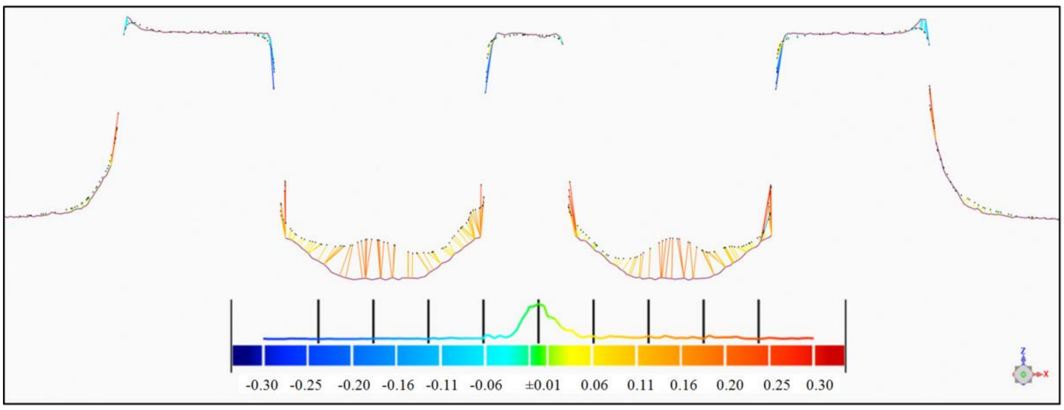

Figure 10: 2D-comparison carried out for "Section 2" of Pyramid 1. The color scale is expressed in millimeters.

The maximum 2D-deviation has been calculated in correspondence of the maximum depth of the holes and is about 0.150 mm. Since the hole is 1.3 mm depth (Table 1), this value represents a percentage error of 11.5% respect to the nominal value. It is important to notice, however, that with the conoscopic holography technology is not possible to scan vertical walls and therefore, the profile of some sections are incomplete. On the contrary, photogrammetric technique returns a complete information of the profile of the considered feature (Figure 11).

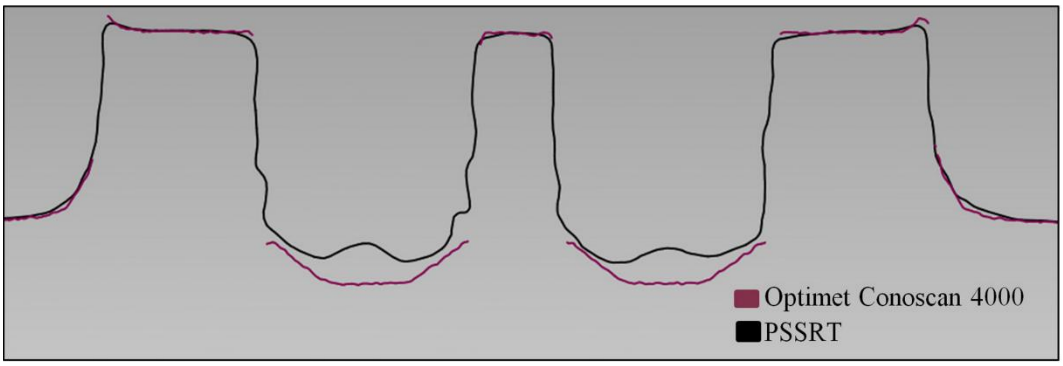

Figure 11: Comparison of the curves of Pyramid 1 calculated in Section2.

Finally 2D measurements were performed with the OC 4000 and the PSSRT and compared. The differences of the data are within 0 – 0.009 mm (Table 6). The measurements were not carried out for Pyramid 4 since the step height of this sample is 0.002 mm (Table 1) and at this scale, the phenomenon of the elastic recovery of the material after the passage of the tool strongly affects the profile of the machined surface [33]. As can be seen in Figure 12 the horizontal profile of each step is not perfectly parallel to the X axis and it is very difficult to distinguish the points relative to the horizontal profile of a step, from those relative to the adjacent steps, that makes very difficult to measure the step height with low uncertainty.

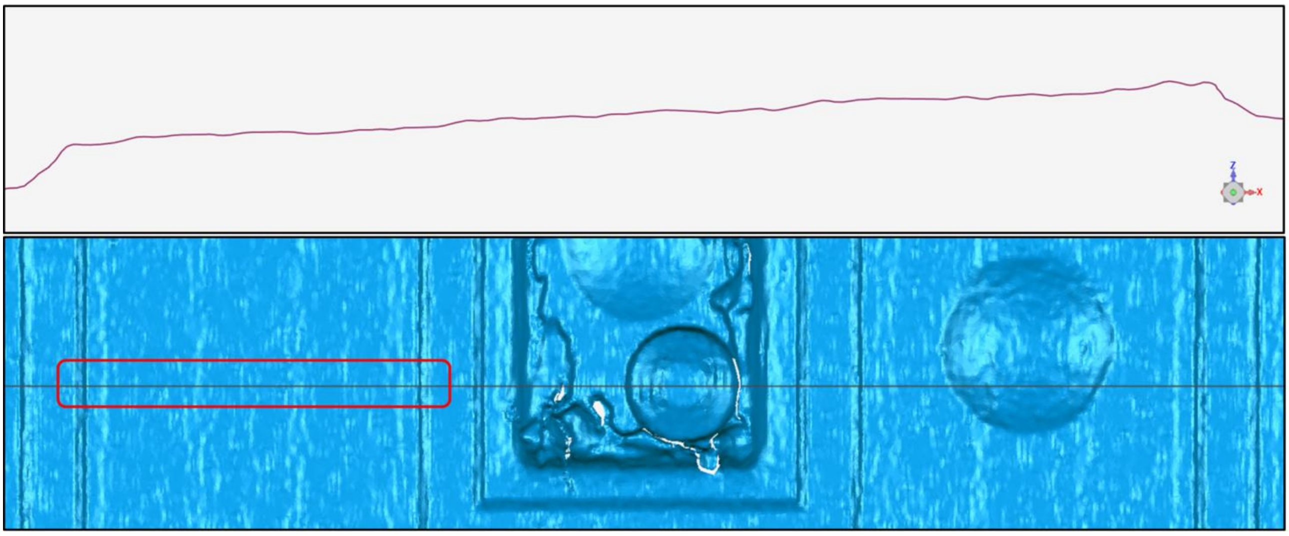

Figure 12: Portion of the curve obtained by sectioning the 3D digital model of Pyramid 1 obtained with Optimet™ Conoscan 4000.

Conclusions and future work

This work demonstrates that it is possible to develop a powerful, precise, rapid and cost effective scanner suitable to scan small parts with complex surfaces and sub-millimeter features. Contrary to what is stated in [7], the photogrammetric technique has proved to be suitable to realize precise 3D digital models for these small parts. This was also demonstrated in some recent works [20,21], but in the present article significant improvements in terms of shooting technique, acquisition times, quality and precision of measurements are presented.

The results are remarkable and the analyses carried out for the four benchmarks, have highlighted the precision of the 3D digital models obtained with the proposed PSSRT respect to those obtained with Optimet™ Conoscan 4000. The proposed PSSRT has proved to be performing and suitable to scan the well-lit areas such as the edges of the steps. From the other side, the 3D-comparisons and 2D-comparisons highlighted a weakness related to the difficulty to obtain a good reconstruction of the poorly lit areas such as the interior of deep holes. Further efforts should be carried out in order to improve the lightening system and resolve the issues related to the scan of problematic features such as deep holes. Moreover, a thorough study on the internal and external calibration process of the measuring instrument, should be conducted in order to eliminate any distortions in the model as well as the need to scale the digital model through an additional measuring instrument.

Acknowledgement

This research is funded by the Italian Ministry of Instruction, University and Research, project PON02_00576_3333604, named "INNOVHEAD- “Innovative technologies for reducing emissions, fuel consumption and operating costs of heavy duty engines”, Activity 9.5:" Dimensional control with 3D scanning with micrometer accuracy".

Bibliography

[1] Byrne G, Dornfeld D, Denkena B. Advancing cutting technology. CIRP Ann - Manuf Technol 2003;52(2):483–507.

[2] Malek CK, Saile V. Applications of LIGA technology to precision manufacturing of high-aspect-ratio micro-components and -systems: a review. Microelectronics J 2004;35(2):131 – 143.

[3] Qin Y, Brockett A, Ma Y, Razali A, Zhao J, Harrison C, et al. Micro-manufacturing: research, technology outcomes and development issues. Int J Adv Manuf Technol 2009;47(9-12):821 – 837.

[4] Mohan S, Mishra RS. Friction stir microforming of superplastic alloys. Microsyst Technol 2005;11(4-5):226 – 229.

[5] Bauer W, Knitter R, Emde A, Bartelt G, Göhring D, Hansjosten E. Replication techniques for ceramic microcomponents with high aspect ratios. Microsyst Technol 2002;9(1-2):81 – 86.

[6] Hansen HN, Carneiro K, Haitjema H, De Chiffre L. Dimensional Micro and Nano Metrology. CIRP Ann - Manuf Technol 2006;55(2):721 – 743.

[7] Savio E, De Chiffre L, Schmitt R. Metrology of freeform shaped parts. CIRP Ann - Manuf Technol 2007;56(2):810 – 835.

[8] Dierick M, Van Hoorebeke L, Jacobs P, Masschaele B, Vlassenbroeck J, Cnudde V, et al. The use of 2D pixel detectors in micro- and nano-CT applications. Nucl Instruments Methods Phys Res Sect A Accel Spectrometers, Detect Assoc Equip 2008;591(1):255 – 259.

[9] Fisher RF, Hintenlang DE. Micro-CT Imaging of MEMS Components. J Nondestruct Eval 2008;27(4):115 – 125.

[10] Ho ST, Hutmacher DW. A comparison of micro CT with other techniques used in the characterization of scaffolds. Biomaterials 2006;27(8):1362 –1376.

[11] Wu Z, Li Z, Huang W, Gong H, Gao Y, Deng J, et al. Comparisons of nozzle orifice processing methods using synchrotron X-ray micro-tomography. J Zhejiang Univ Sci A 2012;13(3):182 – 188.

[12] Amenabar I, Mendikute A, López-Arraiza A, Lizaranzu M, Aurrekoetxea J. Comparison and analysis of non-destructive testing techniques suitable for delamination inspection in wind turbine blades. Compos Part B Eng 2011;42(5):1298 – 1305.

[13] Yang P, Takamura T, Takahashi S, Takamasu K, Sato O, Osawa S, et al. Development of high-precision micro-coordinate measuring machine: Multi-probe measurement system for measuring yaw and straightness motion error of XY linear stage. Precis Eng 2011;35(3):424 – 430.

[14] Goo C-S, Jun MBG, Saito A. Probing system for measurement of micro-scale components. J Manuf Process 2012;14(2):174–80.

[15] Fan KC, Fei YT, Yu XF, Chen YJ, Wang WL, Chen F, et al. Development of a low-cost micro-CMM for 3D micro/nano measurements. Meas Sci Technol 2006;17(3):524 – 532.

[16] Meli F, Küng A. AFM investigation on surface damage caused by mechanical probing with small ruby spheres. Meas Sci Technol 2007;18(2):496 – 502.

[17] Vliet WP Van, Schellekens PH. Accuracy limitations of fast mechanical probing. CIRP Ann - Manuf Technol 1996;45(1):483 – 487.

[18] Hoffmann J, Weckenmann A, Sun Z. Electrical probing for dimensional micro metrology. CIRP J Manuf Sci Technol 2008;1(1):59 – 62.

[19] Schwenke H, Neuschaefer-Rube U, Pfeifer T, Kunzmann H. Optical methods for dimensional metrology in production engineering. CIRP Ann - Manuf Technol 2002;51(2):685 – 699.

[20] Nguyen C, Lovell D, Oberprieler R, Jennings D, Adcock M, Gates-Stuart E, et al. Virtual 3D Models of Insects for Accelerated Quarantine Control. 2013 IEEE Int. Conf. Comput. Vis. Work., IEEE; 2013, p. 161 – 167.

[21] Nguyen C V, Lovell DR, Adcock M, La Salle J. Capturing natural-colour 3D models of insects for species discovery and diagnostics. PLoS One 2014;9(4):e94346.

[22] Galantucci LM, Lavecchia F, Percoco G. Multistack Close Range Photogrammetry for Low Cost Submillimeter Metrology. J Comput Inf Sci Eng 2013;13(4):044501.

[23] Galantucci L, Percoco G, Ferrandes R. Accuracy issues of digital photogrammetry for 3D digitization of industrial products. Rev Int D'ingénierie Numérique 2006;2(1-2):29 – 40.

[24] Sinram O, Ritter M, Kleindick S, Schertel A, Hohenberg H, Albertz J. Calibration of an SEM, using a nano positioning tilting table and a microscopic calibration pyramid. Int Arch Photogramm Remote Sens Spat Inf Sci 1976;34(5):210 – 215.

[25] Ritter M, Hemmleb M, Faber P, Lich B, Hohenberg H. SEM/FIB stage calibration with photogrammetric methods. ISPRS Comm. V Symp, 2006.

[26] Ritter M, Hemmleb M, Sinram O, Albertz J, Hohenberg H. A versatile 3D calibration object for various micro-range measurement methods. Proc. XXth ISPRS Congr. Istanbul, 2004, p. 696–701.

[27] Hemmleb M, Albertz J, Schubert M, Gleichmann A, Köhler J. Digital microphotogrammetry with the scanning electron microscope. Int Arch Photogramm Remote Sens 1996;31:225 – 230.

[28] Hemmleb M, Albertz J. Microtopography-The photogrammetric determination of friction surfaces. Int Arch Photogramm Remote Sens 2000;33:56 – 63.

[29] Koutsoudis, A., Vidmar, B., Ioannakis, G., Arnaoutoglou, F., Pavlidis, G., & Chamzas, C. (2014). Multi-image 3D reconstruction data evaluation. Journal of Cultural Heritage, 15(1), 73-79.

[30] Lowe, D. G. (2004). Distinctive image features from scale-invariant keypoints.International journal of computer vision, 60(2), 91-110.

[31] Agisoft PhotoScan User Manual: Professional Edition, Version 1.0.4, 2014, copyright Agisoft LLC.

[32] Optimet. Our Technology Collinear Sensors Optimet n.d. http://www.optimet.com/our_technology.php (accessed October 03, 2014).

[33] Dornfeld D, Min S, Takeuchi Y. Recent advances in mechanical micromachining. CIRP Ann - Manuf Technol 2006;55(2):745 – 768.

Appendix

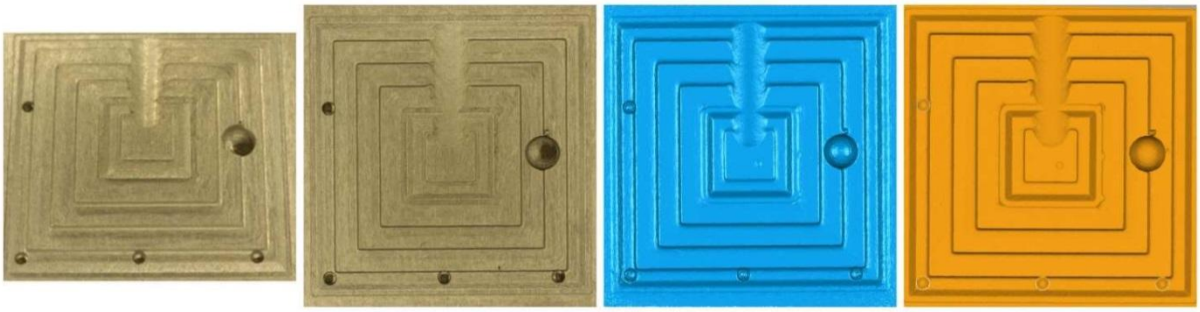

Figure A1: Images related to Pyramid 2: (a) Perspective picture, (b) Texturized 3D digital model obtained with PSSRT, (c) non-texturized 3D digital model obtained with PSSRT, (d) 3D digital model obtained with Optimet™ Conoscan 4000.

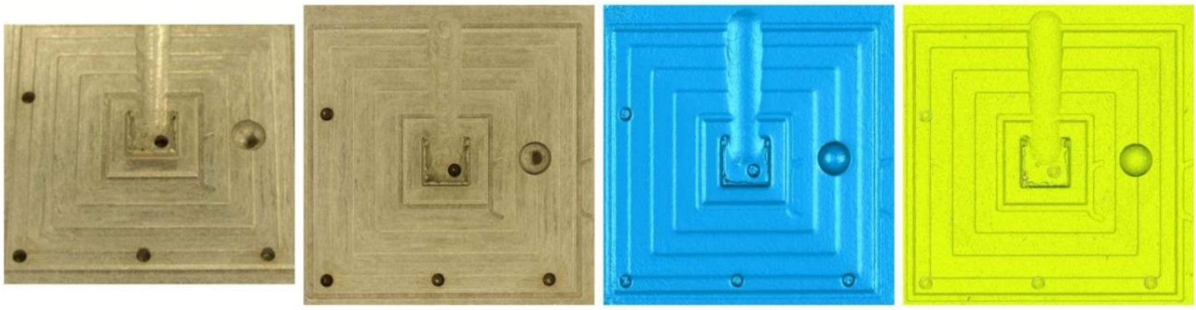

Figure A2: Images related to Pyramid 3: (a) Perspective picture, (b) Texturized 3D digital model obtained with PSSRT, (c) non-texturized 3D digital model obtained with PSSRT, (d) 3D digital model obtained with Optimet™ Conoscan 4000.

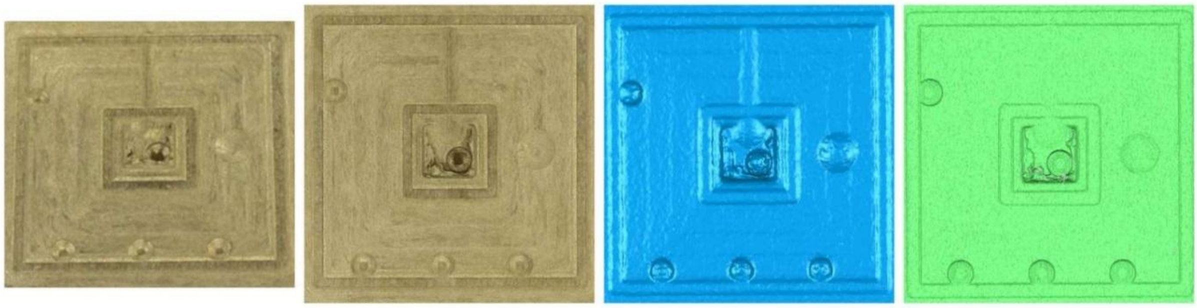

Figure A3: Images related to Pyramid 4: (a) Perspective picture, (b) Texturized 3D digital model obtained with PSSRT, (c) non-texturized 3D digital model obtained with PSSRT, (d) 3D digital model obtained with Optimet™ Conoscan 4000.

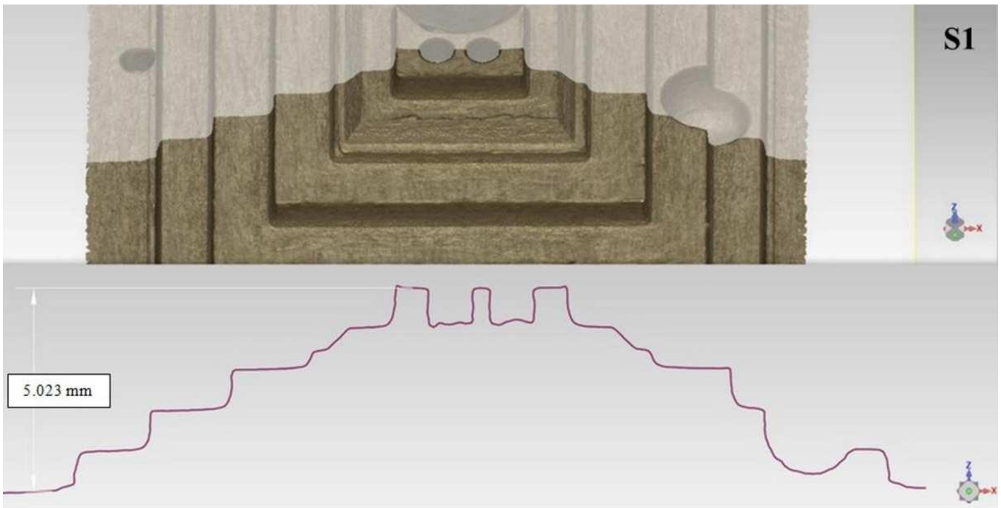

Figure A13: Section S1 of the 3D digital model of Pyramid 1 and measurement of the feature F1.

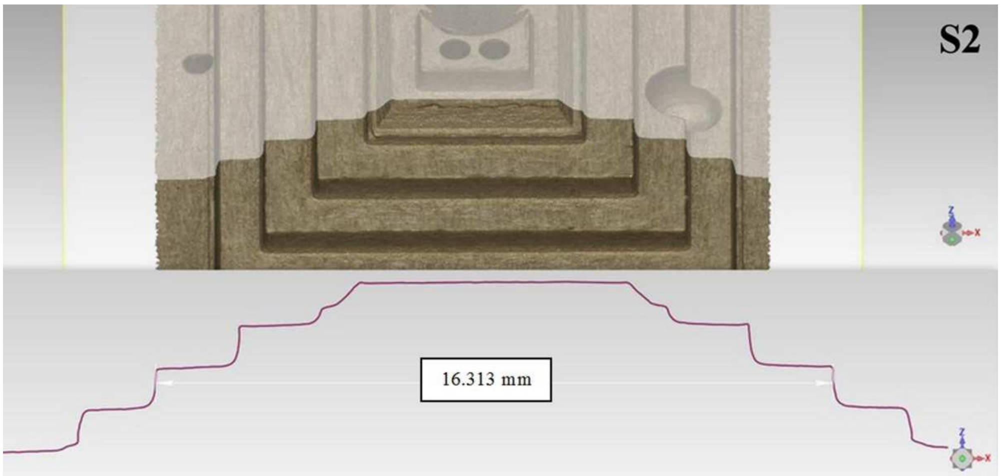

Figure A5: Section S2 of the 3D digital model of Pyramid 1 and measurement of the feature F2.

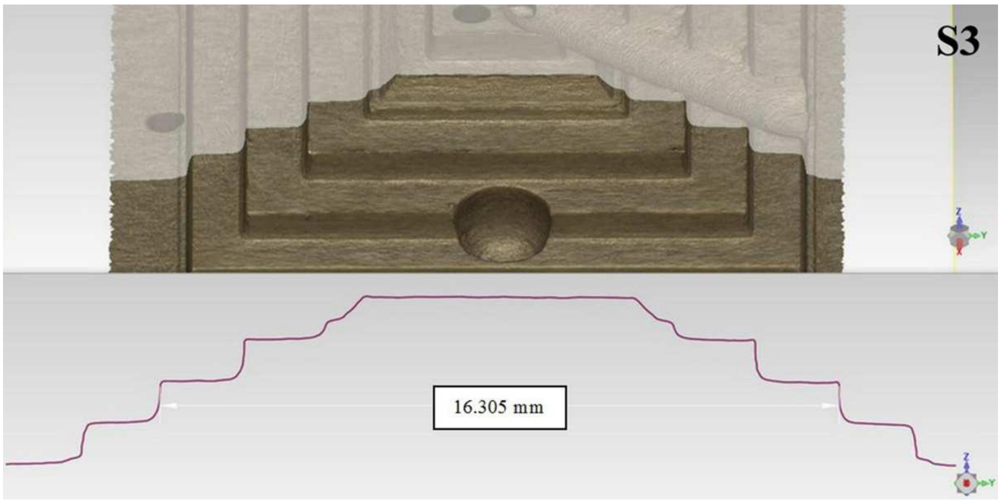

Figure A6: Section S3 of the 3D digital model of Pyramid 1 and measurement of the feature F3.